

Multipole conservation laws and subdiffusion in any dimension

Jason Iaconis,¹ Andrew Lucas,¹ and Rahul Nandkishore¹

¹*Department of Physics and Center for Theory of Quantum Matter,
University of Colorado, Boulder, Colorado 80309, USA*

(Dated: September 15, 2020)

Subdiffusion is a generic feature of chaotic many-body dynamics with multipole conservation laws and subsystem symmetries. We numerically study this subdiffusive dynamics, using quantum automaton random unitary circuits, in a broad range of models including one dimensional models with dipole and quadrupole conservation, two dimensional models with dipole conservation, and two dimensional models with subsystem symmetry on the triangular lattice. Our results are in complete agreement with recent hydrodynamic predictions for such theories.

I. INTRODUCTION

Understanding the dynamics of closed quantum systems in the presence of symmetry is an important problem which has broad implications for our understanding of thermalization in quantum many-body systems [1, 2]. Random quantum circuit models offer a clean platform where such dynamics can be studied [3–8]. In theories with $U(1)$ symmetry, such quantum circuit models readily reproduce the expected diffusive dynamics predicted by Fick’s law [9, 10]. Qualitatively new behavior can emerge, however, when one looks at models with unconventional conservation laws and symmetries. Two important examples of this are: (1) systems where both total charge and the total dipole moment (or even higher multipole moments) of the charge are conserved, and (2) systems with *subsystem symmetry*, where total charge is independently conserved along intersecting subdimensional sublattices. Such unusual conservation laws are motivated by the dynamics of fracton systems [11–16] but may also be realized in more conventional settings [17, 18].

Implementation of these types of symmetries in local random circuits has led to the discovery of unique dynamical phenomena, such as the existence of charge localization [17, 19, 20] in certain (exponentially large) subspaces, and anomalous subdiffusion outside them [21]. In [18], a hydrodynamic theory was formulated, which describes the late time and long wavelength behavior of the charge density. This hydrodynamic theory is valid in almost all states, outside of the localized subspace (whose measure is exponentially small in system size for “generic” models). These analytic predictions were numerically confirmed in [22, 23], and analytically in certain large- N models [24, 25].

In this paper, we numerically test the analytic predictions of [18] in a much larger family of models. In particular, we study 1D circuits with both dipole and quadrupole conservation, 2D square lattice circuits with dipole conservation, and 2D triangular lattice circuits with non-orthogonal subsystem symmetry. Throughout we use the numerical method from [21], which allows us to numerically simulate the dynamics for very large system sizes and very long circuit depths. We probe the dynamics

through the dynamical evolution of wave functions with special initial charge configurations. This allows us to excite isolated long wavelength modes so that we can directly compare with the field theoretic results of [18]. In every case, the numerical results are in agreement with analytic expectations.

II. AUTOMATON DYNAMICS

The numerical method we employ is based on quantum automaton circuits [21, 26, 27]. Cellular automaton dynamics are defined as any unitary evolution which does not generate entanglement in an appropriate basis. Under an automaton gate, U , an initial computational basis state $|m\rangle$ becomes

$$U|m\rangle = e^{i\theta_m}|\pi(m)\rangle. \quad (1)$$

where $\pi \in S_D$ is an element of the permutation group on the D elements which form the computational basis states. If we start with an arbitrary initial state

$$|\psi_0\rangle = \sum_m c_m |m\rangle, \quad (2)$$

we have

$$U|\psi_0\rangle = \sum_m c_m e^{i\theta_m} |\pi(m)\rangle \quad (3)$$

For computational basis states, $|m\rangle$, no entanglement is generated by the dynamics and we can therefore exactly track the evolution of $|m(t)\rangle$. While the evolution of a single computational basis state $|m\rangle$ is fully classical, it is important to note that automaton circuits do generate volume law entanglement when acting on product states which are *not* initially in the computational basis. Further, as explained extensively in [21], automaton dynamics generically generate volume law operator entanglement, which allows us to numerically study the hydrodynamics of operator spreading. In all cases, we are able to simulate the dynamics classically by Monte Carlo sampling random states $|m\rangle$ and tracking the evolution as in Eq. 1. When using this to evolve operators or arbitrary initial states, this protocol amounts to a type of quantum Monte Carlo.

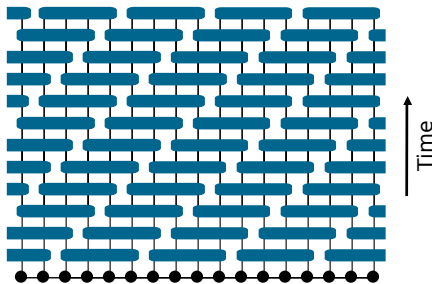


FIG. 1. The random circuit architecture used for 1D circuits. Each site contains a 3 state qudit, and the automaton gates of size $|G|$ (shown here for $|G| = 4$), randomly permute the charge configurations in a way which is consistent with the symmetry constraints. A similar architecture is used for 2D circuits with gates of size $|G| = G_x \times G_y$, with successive layers shifted by one site in the x -direction for G_x layers followed by a single site shift in the y -direction. Examples of allowed charge permutations are shown in Fig. 2.

Let us contrast the automaton method with earlier numerical methods, which were largely based instead on simulating Haar random circuits [9, 10, 17, 19, 20]. Here, one constructs local unitary matrices which are block diagonal in each symmetry sector, but for which each block is chosen to be Haar random. This approach is possible for small systems, and has been performed in studies with very simple symmetry constraints. However, for the constrained dynamics of interest in this paper, Haar random circuits quickly become intractable for systems whose on-site Hilbert space dimension is larger than 2, and/or which have many more than 10-20 lattice sites. Moreover, in the case of higher-moment conserving dynamics, very large systems are required to observe the correct quantitative behavior. This is why we use the automaton dynamics.

Despite their apparent simplicity, automaton circuits appear to produce generic chaotic dynamics [21, 28]. We expect that essentially any property of a generic Haar random unitary dynamics can also be seen in a corresponding automaton circuit, as long as we choose appropriate initial conditions.

In this work, we will mainly focus on the evolution of spin-1 wave functions $|\psi_0\rangle = \sum_m c_m |m\rangle$, $|m\rangle \in \{|+\rangle, |0\rangle, |-\rangle\}$, where the coefficients c_m are chosen to induce a net multipole moment. We then apply a random local unitary circuit $U = \prod_{i,t} U_{i,t}$, composed of local unitary gates of size $|G|$ as shown in Fig. 1. The gates $U_{i,t}$ perform a random permutation of the spins within the block diagonal symmetry sector consistent with the charge and multipole conservation laws.

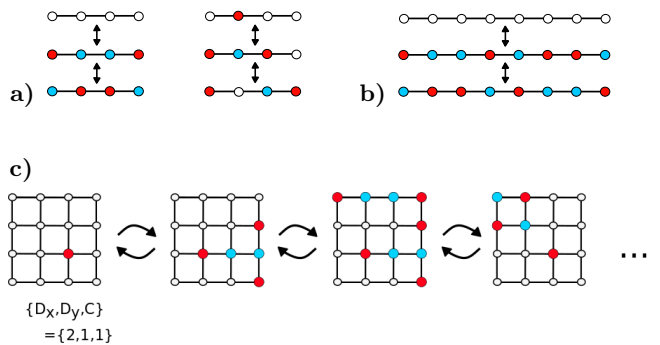


FIG. 2. Examples of allowed charge permutations for **a)** 4 site 1D gates with dipole conservation, **b)** 8 site 1D gates with quadrupole conservation and **c)** 2D 4x4 unitary gates with dipole conservation in both the x and y directions.

III. 1D CIRCUITS WITH DIPOLE CONSERVATION

We first simulate 1D circuits with dipole conservation laws using the method of [21]. This is an extension of the numerical analysis of [22], where the auto-correlation function $\langle S^z(x,t)S^z(x,0) \rangle$ was studied and was found to decay sub-diffusively. In this work, we also present the Fourier correlators $\langle S^z(k,t)S^z(k,0) \rangle$, and explicitly demonstrate the exponential decay of hydrodynamic modes predicted by [18]. The local charge density in dipole conserving systems obeys the equation of motion [18, 29]

$$\partial_t \rho + \partial_i \partial_j J_{ij} = 0. \quad (4)$$

Hydrodynamics implies that in one dimension

$$J_{xx} = B_1 \partial_x^2 \rho. \quad (5)$$

The decay rate of the Fourier correlator is then

$$C(k,t) = \langle S^z(k,t)S^z(k,0) \rangle \sim \exp[-Bk^4 t]. \quad (6)$$

This then implies the autocorrelator

$$G(t) = \langle S_i^z(x,t)S_i^z(x,0) \rangle \sim t^{-1/4}. \quad (7)$$

In Fig. 3, as in [22], we see that the decay indeed follows this scaling form very closely.

We now would like to more directly probe the equation of motion Eq. 4, by studying the relaxation rate of specific charge modes. To do this, we simulate the dynamics of the spin-1 state

$$|\psi_0\rangle = \frac{1}{\mathcal{N}} \otimes |\vec{h}_i\rangle \quad (8)$$

$$|\vec{h}_i\rangle = (1 + h_i)|+\rangle + |0\rangle + (1 - h_i)|-\rangle \quad (9)$$

$$h_i = \begin{cases} |h| & \text{if } x \leq \frac{L}{4} \text{ or } x \geq \frac{3L}{4} \\ -|h| & \text{if } \frac{L}{4} < x < \frac{3L}{4} \end{cases},$$

where \mathcal{N} is a normalization factor. That is, we simulate the dynamics of a wave function with zero net charge and

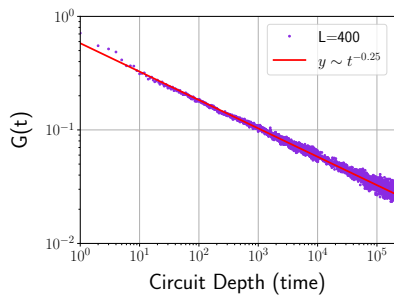


FIG. 3. We measure the autocorrelation time for 1D circuits with dipole conservation. The slow relaxation rate at the long wavelengths gives an anomalously slow decay of $G(t) = \langle S^z(x, t) S^z(x, 0) \rangle$. In this case we see that $G(t) \sim t^{-0.25}$.

dipole moment, but with a finite quadrupole moment. The charge is configured in a square wave of the form $|+-+ \rangle$, with wavelength $\lambda = L$.

The value of the field $|h|$ is adjusted so that the net charge in each quadrant of the lattice is the same for different system sizes. At long times, the state will relax to a fully neutral state. We then measure the net charge in region $A = \{x < \frac{L}{4}\}$ as a function of time, and therefore measure the relaxation rate for charge modes $k = \frac{2\pi}{L}$. We expect the charge to decay exponentially, as in (6). The results are shown in Fig. 4 a), where we simulated circuits with gates of size $|G| = 8$. We find that all curves collapse onto the universal function

$$C(t, L) = F\left(\frac{t}{L^4}\right). \quad (10)$$

Note that to see this data collapse, we must simulate circuits to a depth, D , which scales with system size like $D \sim L^4$. For the largest systems we simulate, we have $L = 320$, and go up to depths $D \sim 2.0 \times 10^7$. We therefore see the benefit of performing the simulation using automaton circuits, which allow us to efficiently study such large system sizes and extreme circuit depths.

In Fig. 4 b), we looked at the dependence of the relaxation rate on gate size. We know that for sufficiently small gate size, the Hilbert space for quantum circuits with multipole conservation laws will exhibit ‘strong shattering’ [17, 20] and that the system will not thermalize at all. For dipole conserving circuits, it is known that gates of size $|G| = 4$ are needed for thermalization to occur. In the limit of large gate size we might expect that

$$C(t, L) = F\left[t\left(\frac{|G|}{L}\right)^4\right]. \quad (11)$$

Our results confirm this scaling form. The data appears to collapse onto a universal function for $|G| > 5$. For $|G| = 4$, the charge still decays, however the relaxation rate appears to be far slower. This short wavelength effect is likely due to the shattering of the Hilbert space which is more extreme for smaller gate sizes.

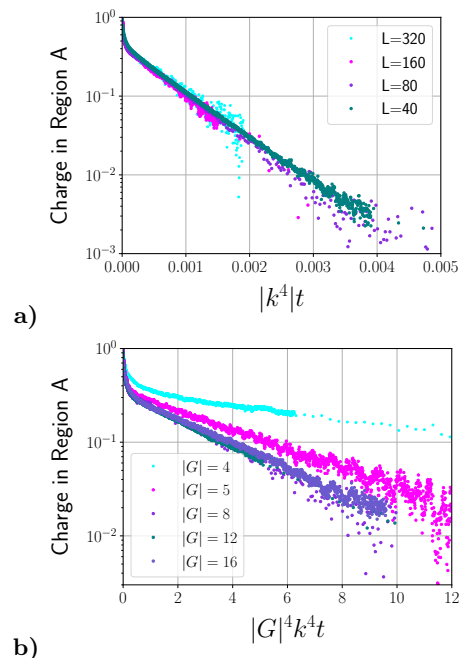


FIG. 4. **a)** The dissipation time for the 1D dipole conserving circuit with gates of size $|G| = 8$, starting from an initial square wave state with wavelength L . The charge in the region $A = \{x < \frac{L}{4}\}$ decays exponentially with a relaxation rate τ which depends on the wavelength k of the initial state. Note that the time axis is scaled by the system size to the fourth power t/L^4 , indicating that the longest wavelength mode relaxes like $\tau \sim k^4$. **b)** The charge dissipation for the same system as a function of gate size $|G|$ eventually collapses onto a universal function when the time axis is scaled like $t(|G|/L)^4$.

IV. 1D CIRCUITS WITH QUADRUPOLE CONSERVATION

We now extend these results to 1D circuits with quadrupole conservation laws. Much of the analysis remains the same as the case with dipole conservation. The equation of motion governing the time evolution of the charge density now includes an additional two factors of the spatial derivative:

$$\partial_t \rho - B \partial_x^6 \rho = 0, \quad (12)$$

which in turn implies that density modulations at wave number k relax in time $\tau \sim k^6/B$.

To see this behavior in our lattice model, we now simulate the evolution of an initial wave function with a net zero quadrupole moment, but a nonzero long wavelength octopole moment.

$$|\psi_0\rangle = \frac{1}{\mathcal{N}} \otimes |\vec{h}_i\rangle \quad (13)$$

$$|\vec{h}_i\rangle = (1 + h_i)|+\rangle + |0\rangle + (1 - h_i)|-\rangle \quad (14)$$

$$h_i = \begin{cases} |h| & \text{if } x \in A \\ -|h| & \text{if } x \in B \end{cases},$$

where \mathcal{N} is a normalization factor and the regions A and

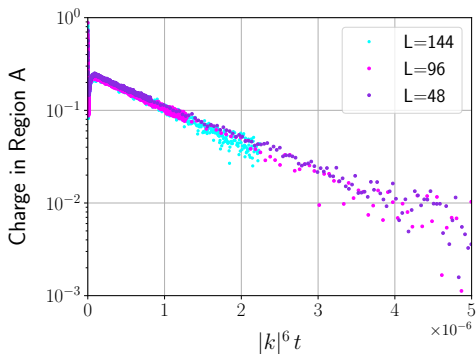


FIG. 5. Dissipation time for different system sizes in the quadrupole conserving circuit. Note that all curves collapse onto a universal function of $\exp(-ct/L^6)$, showing that the relaxation rate scales like $\tau \sim k^6$

B are defined as

$$A = \left[0, \frac{L}{8}\right] \cup \left[\frac{3L}{8}, \frac{L}{2}\right] \cup \left[\frac{5L}{8}, \frac{7L}{8}\right] \quad (15)$$

$$B = \left[\frac{L}{8}, \frac{3L}{8}\right] \cup \left[\frac{L}{2}, \frac{5L}{8}\right] \cup \left[\frac{7L}{8}, L\right]. \quad (16)$$

We measure the relaxation time in these states, using circuits with gates of size $|G| = 12$.

The results are shown in Fig. 5. We see that the data collapses onto the universal function

$$C(t, L) = C(0)F\left(\frac{t}{L^6}\right). \quad (17)$$

and that the decay is exponential in time. This implies that charge relaxes like $\tau \sim e^{-k^6 t}$.

Again, the system sizes we are able to study are limited by the circuit depths that can be simulated in a reasonable amount of time. In this case, the circuit depth must scale like $D \sim L^6$. The largest systems we simulated contained $L = 144$ and again went to depths $D = 2 \times 10^7$.

V. 2D CIRCUITS WITH DIPOLE CONSERVATION

We now turn our attention to studying multipole conservation in 2D systems. This is a case not studied in previous literature [21, 22]. The equations (4)-(5) continue to hold. However, in two dimensions and on a square lattice, the allowed tensor structures in J_{ij} are non-trivial:

$$J_{ij} = -[B_1 \delta_{ijkl} + B_2 \delta_{ij} \delta_{kl} + B_3 \delta_{ik} \delta_{jl}] \partial_k \partial_l \rho \quad (18)$$

where $\delta_{ijkl} = \delta_{ij} \delta_{ik} \delta_{il}$ demands all 4 indices are the same. Hence we predict that

$$C(k, t) = C(k, 0) \exp[-D(k_x, k_y)t] \quad (19)$$

$$D(k_x, k_y) = D_{ijkl} k_i k_j k_k k_l, \quad (20)$$

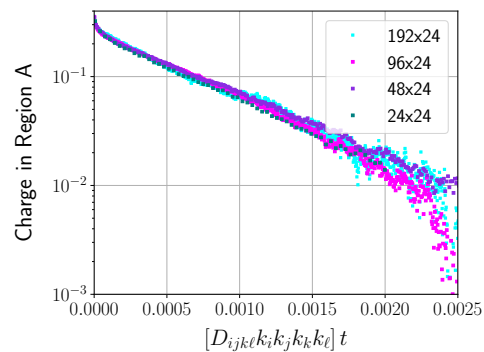


FIG. 6. Dissipation time for the 2D dipole conserving model. All curves collapse onto a universal function $\exp(-D_{ijkl} k_i k_j k_k k_l t)$ with $\{k_x, k_y\} = \{\frac{2\pi}{L_x}, \frac{2\pi}{L_y}\}$. The form of the tensor D_{ijkl} is given in Eq. 21. We see that the relaxation rate generically scales like $\tau \sim |k|^4$. We simulate the charge relaxation for systems with different aspect ratios. This allows us to fit the degree of anisotropy introduced by the square lattice, by fitting with the parameter defined in Eq. 22.

where

$$D_{ijkl} k_i k_j k_k k_l = (B_2 + B_3)(k_x^2 + k_y^2)^2 + B_1(k_x^4 + k_y^4). \quad (21)$$

Of most interest is the ratio

$$b = -\frac{B_1}{B_2 + B_3} \quad (22)$$

which encodes the level of anisotropy due to the square lattice. We can determine b by looking at the relaxation rate for systems with different aspect ratios $R = L_x/L_y$.

We simulate the 2D model for various aspect ratios, using gates of size $|G| = 4 \times 4$. Using these relatively large gate sizes allows the charge to decay more quickly, easing the computational burden of the simulation since extreme circuit depths are not needed. Some examples of allowed charge configurations are shown in Fig. 2, whereby a local charge can move by emitting an x or y dipole. Charge configurations with a net-zero dipole moment can also be created from the vacuum state within the 4×4 sublattice.

We initialize our wave function to have a net zero dipole moment but a finite quadrupole moment by dividing the lattice into four quadrants and inducing a positive (negative) net charge in the lower left and upper right (lower right and upper left) quadrants.

The results of our 2D simulation are shown in Fig. 6. The optimal data collapse occurs with $b \sim 0.8$, where b is defined as in Eq. 21. We find that, in this case, the long wavelength modes indeed decay like $|k|^4$.

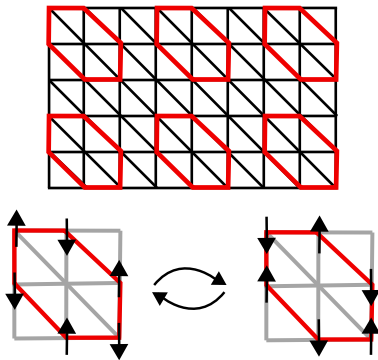


FIG. 7. The skewed triangular lattice, which is equivalent to the actual triangular lattice under the discrete circuit dynamics. The smallest non-trivial gate which preserves the subsystem symmetry acts nontrivially on the 6 sites of the hexagons shown here. Note that each unit cell consists of 9 sites, but the gates act trivially on 3 of these sites. The subset of nontrivial configurations is shown below. Such a tiling pattern would be repeated and shifted to begin at all sites of the unit cell, so that one timestep is equal 9 layers of the circuit

VI. SUBSYSTEM SYMMETRY ON THE TRIANGULAR LATTICE

Lastly, we look at a different example of a higher order conservation law: subsystem symmetries. As mentioned earlier, subsystem symmetry occurs when a lower dimensional symmetry is embedded in a higher dimensional system. In our case, we look at systems where charge is conserved on each row of the lattice individually. On the square lattice and cubic lattice, this was studied in Ref. 21, where subdiffusive behavior was found. Here, we extend this analysis to the case of *nonorthogonal* subsystem symmetries. In particular, we look at a triangular lattice system, where charge is conserved on each row of the triangular lattice.

In this case, unlike the rest of the paper, we study a spin-1/2 system. The subsystem symmetry can be implemented in an automaton circuit by applying a gate which acts on a 3×3 sublattice and flips between two specific charge configurations, illustrated in Fig. 7. We then obtain a conserved charge along all lattice directions $\vec{\lambda}_k$: for any starting point \mathbf{x} and lattice direction \mathbf{e}_k ,

$$Q_{k,\mathbf{x}} = \sum_n S_{\mathbf{x}+n\mathbf{e}_k}^z \quad (23)$$

is conserved. (Note that these are not all unique charges, as defined above.)

We expect that for the triangular lattice, [18]

$$\partial_t G(x, t) = -\lambda \partial_{a_1}^2 \partial_{a_2}^2 \partial_{a_3}^2 G(x, t). \quad (24)$$

where ∂_{a_i} denotes the derivative along the i -th lattice direction and $G(x, t) = \langle S^z(x, t) S^z(0, 0) \rangle$. In general, if there are n linear constraints we might find

$$\partial_t G(x, t) = (-1)^{n+1} \lambda \partial_{a_1}^2 \partial_{a_2}^2 \dots \partial_{a_n}^2 G(x, t). \quad (25)$$

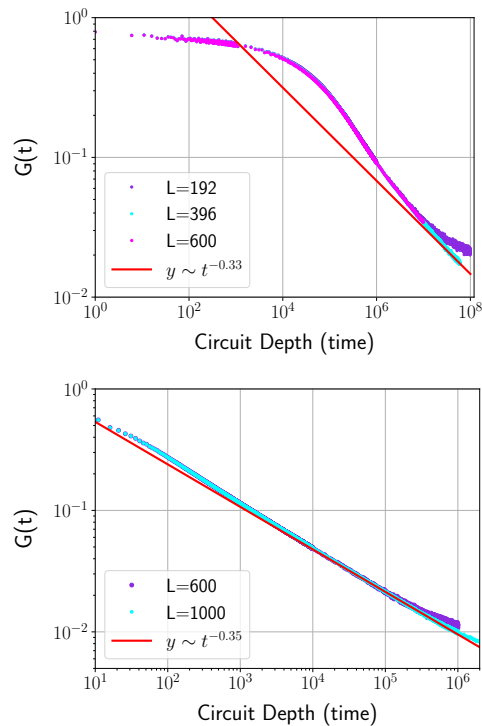


FIG. 8. The 2D triangular lattice autocorrelation function. (*top*) For the circuit with the smallest fundamental gates (3×3 gates), there are at least two regimes. At relatively short times, the scaling is very slow, $G(t) \sim t^{-\alpha}$ with $\alpha \ll \frac{1}{3}$. The scaling then slows down at very long times, and in this regime it appears to approach the predicted value $G(t) \sim t^{-1/3}$. (*bottom*) When gates of dimension 4×4 are used, the relaxation to the power law scaling regime is much faster. Here, we see a fit at late times to the form $G(t) \sim t^{-0.350(2)}$. This exponent is very close to the predicted value of $\frac{1}{3}$. We expect that for even larger systems and later times, the power law decay will converge to this predicted value.

Going back to the triangular lattice case, we expect that the real space autocorrelation function is then

$$G(r, t) \sim \int d^2 k e^{i\mathbf{k}r - \lambda k_{a_1}^2 k_{a_2}^2 k_{a_3}^2 t} \quad (26)$$

$$= \int d^2 k' e^{i\mathbf{k}'r \cos \theta - \lambda k'^6 t \sin^2(3\theta)}. \quad (27)$$

In the second equation we have switched to polar coordinates in wave number space. Setting $r = 0$ for simplicity, we find

$$G(0, t) \sim (\lambda t)^{-1/3} \int \frac{d\theta}{|\sin(3\theta)|^{2/3}} \sim t^{-1/3}. \quad (28)$$

Note that on a square lattice where $\sin(3\theta)$ is replaced by $\sin(2\theta)$ and k^6 is replaced by k^4 , there is a logarithmic correction coming from a divergent θ integral above.

We now numerically calculate this autocorrelation function. The results are shown in Fig. 8. For gates of size 3×3 , the autocorrelation function takes a very

long time to reach the final scaling regime. Before this, the charge appears to go through a regime where the decay is very slow. The origin of this non-hydrodynamic effect is not understood. For gates of size 4×4 , the decay rapidly approaches the hydrodynamic predictions above.

VII. DISCUSSION

We have tested the analytic predictions of hydrodynamics [18] for subdiffusion in multipole conserving systems numerically, using a numerical method from [21]. Specifically, we have checked one dimensional systems with dipole and/or quadrupole conservation, two dimensional systems with dipole conservation, and triangular lattice systems with subsystem conservation laws along three non-orthogonal directions. In every case we find results in agreement with the analytic expectations. The numerical tests involve simulations of dynamics for very

large system sizes and times. Our work thus demonstrates both the accuracy of the analytic predictions in [18], and the versatility and utility of the numerical method introduced in [21]. In the future, it would be interesting to extend these simulations to more exotic scenarios, perhaps with reduced spacetime symmetries, or with unconventional interplays between conserved multipoles and other conservation laws such as energy.

ACKNOWLEDGEMENTS

We acknowledge prior collaborations on related work with Andrey Gromov and Sagar Vijay. This material is based upon work supported in part (J.I. and R.N.) by the Air Force Office of Scientific Research under award number FA9550-20-1-0222. A.L. was supported by a Research Fellowship from the Alfred P. Sloan Foundation.

-
- [1] Marcos Rigol, Vanja Dunjko, and Maxim Olshanii, “Thermalization and its mechanism for generic isolated quantum systems,” *Nature* **452**, 854–858 (2008).
 - [2] Rahul Nandkishore and David A. Huse, “Many-body localization and thermalization in quantum statistical mechanics,” *Annual Review of Condensed Matter Physics* **6**, 15–38 (2015), <https://doi.org/10.1146/annurev-conmatphys-031214-014726>.
 - [3] Adam Nahum, Jonathan Ruhman, Sagar Vijay, and Jeongwan Haah, “Quantum entanglement growth under random unitary dynamics,” *Phys. Rev. X* **7**, 031016 (2017).
 - [4] Adam Nahum, Sagar Vijay, and Jeongwan Haah, “Operator spreading in random unitary circuits,” *Phys. Rev. X* **8**, 021014 (2018).
 - [5] A. Nahum, J. Ruhman, and D. A. Huse, “Dynamics of entanglement and transport in 1D systems with quenched randomness,” *Phys. Rev. B* **98**, 035118 (2018).
 - [6] A. Chan, A. De Luca, and J. T. Chalker, “Solution of a minimal model for many-body quantum chaos,” *ArXiv e-prints* (2017), arXiv:1712.06836 [cond-mat.stat-mech].
 - [7] A. Chan, A. De Luca, and J. T. Chalker, “Spectral statistics in spatially extended chaotic quantum many-body systems,” *ArXiv e-prints* (2018), arXiv:1803.03841 [cond-mat.stat-mech].
 - [8] Pavel Kos, Marko Ljubotina, and Tomaž Prosen, “Many-body quantum chaos: Analytic connection to random matrix theory,” *Phys. Rev. X* **8**, 021062 (2018).
 - [9] Vedika Khemani, Ashvin Vishwanath, and David A. Huse, “Operator spreading and the emergence of dissipative hydrodynamics under unitary evolution with conservation laws,” *Phys. Rev. X* **8**, 031057 (2018).
 - [10] Tibor Rakovszky, Frank Pollmann, and C. W. von Keyserlingk, “Diffusive hydrodynamics of out-of-time-ordered correlators with charge conservation,” *Phys. Rev. X* **8**, 031058 (2018).
 - [11] Claudio Chamon, “Quantum glassiness in strongly correlated clean systems: An example of topological overprotection,” *Phys. Rev. Lett.* **94**, 040402 (2005).
 - [12] Jeongwan Haah, “Local stabilizer codes in three dimensions without string logical operators,” *Phys. Rev. A* **83**, 042330 (2011).
 - [13] Sagar Vijay, Jeongwan Haah, and Liang Fu, “A new kind of topological quantum order: A dimensional hierarchy of quasiparticles built from stationary excitations,” *Phys. Rev. B* **92**, 235136 (2015).
 - [14] Sagar Vijay, Jeongwan Haah, and Liang Fu, “Fracton topological order, generalized lattice gauge theory, and duality,” *Phys. Rev. B* **94**, 235157 (2016).
 - [15] Michael Pretko, “Subdimensional particle structure of higher rank $u(1)$ spin liquids,” *Phys. Rev. B* **95**, 115139 (2017).
 - [16] Rahul M Nandkishore and Michael Hermele, “Fractons,” *Annual Review of Condensed Matter Physics* **10**, 295–313 (2019).
 - [17] Vedika Khemani, Michael Hermele, and Rahul Nandkishore, “Localization from hilbert space shattering: From theory to physical realizations,” *Phys. Rev. B* **101**, 174204 (2020).
 - [18] Andrey Gromov, Andrew Lucas, and Rahul M. Nandkishore, “Fracton hydrodynamics,” *Phys. Rev. Research* **2**, 033124 (2020).
 - [19] Shriya Pai, Michael Pretko, and Rahul M. Nandkishore, “Localization in fractonic random circuits,” *Phys. Rev. X* **9**, 021003 (2019).
 - [20] Pablo Sala, Tibor Rakovszky, Ruben Verresen, Michael Knap, and Frank Pollmann, “Ergodicity breaking arising from hilbert space fragmentation in dipole-conserving hamiltonians,” *Physical Review X* **10** (2020), 10.1103/physrevx.10.011047.
 - [21] Jason Iaconis, Sagar Vijay, and Rahul Nandkishore, “Anomalous subdiffusion from subsystem symmetries,” *Phys. Rev. B* **100**, 214301 (2019).
 - [22] Johannes Feldmeier, Pablo Sala, Giuseppe de Tomasi, Frank Pollmann, and Michael Knap, “Anomalous diffusion in dipole- and higher-moment conserving systems,” (2020), arXiv:2004.00635 [cond-mat.str-el].

- [23] Alan Morningstar, Vedika Khemani, and David A. Huse, “Kinetically constrained freezing transition in a dipole-conserving system,” *Phys. Rev. B* **101**, 214205 (2020).
- [24] Pengfei Zhang, “Subdiffusion in strongly tilted lattice systems,” *Physical Review Research* **2**, 033129 (2020).
- [25] Ganesan, Koushik and Lucas, Andrew, “Holographic subdiffusion,” *ArXiv e-prints* (2020), arXiv:2008.09638 [hep-th].
- [26] Sarang Gopalakrishnan and Bahti Zakirov, “Facilitated quantum cellular automata as simple models with non-thermal eigenstates and dynamics,” *Quantum Science and Technology* **3**, 044004 (2018).
- [27] V. Alba, J. Dubail, and M. Medenjak, “Operator entanglement in interacting integrable quantum systems: The case of the rule 54 chain,” *Phys. Rev. Lett.* **122**, 250603 (2019).
- [28] Jason Iaconis, “Quantum state complexity in computationally tractable quantum circuits,” (2020), arXiv:2009.05512 [quant-ph].
- [29] Michael Pretko, “Generalized electromagnetism of sub-dimensional particles: A spin liquid story,” *Phys. Rev. B* **96**, 035119 (2017).